Available online at www.sciencedirect.com
ScienceDirect
Journal of Power Sources 172 (2007) 435–445
JOURNAL OF POWER SOURCES
www.elsevier.com/locate/jpowsour

Study the effect of conductive fillers on a secondary Zn electrode based on ball-milled ZnO and $Ca(OH)_2$ mixture powders

Chun-Chen Yang [a,*], Wen-Chen Chien [a], Ching Li Wang [a], Cheng-Yeou Wu [b]

[a] *Department of Chemical Engineering, Mingchi University of Technology, Taipei Hsien 243, Taiwan, ROC*
[b] *Taiwan Power Research Institute, Taiwan Power Company, Taipei, Taiwan, ROC*

Received 14 May 2007; received in revised form 13 July 2007; accepted 17 July 2007
Available online 2 August 2007

Abstract

The active materials of the secondary Zn electrode containing a mixture powder of zinc oxide (ZnO) and calcium hydroxide ($Ca(OH)_2$) powders were prepared by a ball-milled method. The characteristic properties of active materials of ball-milled ZnO + $Ca(OH)_2$ mixture powders were examined by scanning electron microscopy (SEM) with energy dispersive X-ray (EDX) system, X-ray diffraction (XRD) analysis, and micro-Raman spectroscopy. The prepared Zn powder electrodes were by using the ball-milled active materials powder +2 wt.% highly electronic conductive fillers, i.e., nano-copper or carbon nanotubes (CNTs) powder. The electrochemical properties of the secondary Zn electrodes without and with the conductive fillers were studied by using cyclic voltammetry (CV) and galvanostatic charge/discharge tests. It was found that the charge/discharge properties of the secondary Zn electrode could be improved when the nano-sized conductive fillers were added into the electrode. In fact, it may be due to the formation of a better electronic conduction path in the electrode matrix. In particular, it was found that the best electrochemical properties were the secondary Zn electrode with 2 wt.% nano-copper fillers. According to the results, it is demonstrated here that the CV method is a quick technique to effectively evaluate the performance of a secondary Zn electrode.

Keywords: Secondary Zn electrode; Cyclic voltammetry (CV); Conductive fillers; Nano-sized copper; CNTs

1. Introduction

The secondary alkaline Zn electrode for Zn-air batteries [1–8] has advantages of high specific energy, low cost, and environmental friendliness. However, the use and development for a secondary Zn electrode on rechargeable battery are still limited because of the dendritic growth, shape change, and high solubility of zinc discharge products in concentrated alkaline KOH solution. These problems are responsible for the short cycle life of a Zn electrode and the poor electrochemical performance for secondary batteries. In order to eliminate the Zn dendritic formation, many attempts have been undertaken, including the use of some additive fillers either in the electrode [9–11] or in the electrolyte [12–15]. The secondary Zn electrodes based on the calcium zincate as an active material have been studied [6,16–18]. Calcium zincate ($CaZn_2(OH)_2{\cdot}H_2O$) was obtained by mechanical ball milling of ZnO and $Ca(OH)_2$ in water medium. Since those composite powder oxides have lower solubility in concentrated KOH solution and better charge/discharge reversibility, it can overcome the problems of the shape changes and dendritic formation to enhance the cycle life of the Zn electrode. Yu et al. [18] studied the electrochemical properties of calcium zincate on a secondary Ni–Zn cell by a powder microelectrode, it showed good prospect for practical applications. Zhang et al. [6] also investigated the influence of metallic bismuth powder as an additive and chemically co-precipitated calcium zincate as active material on the secondary electrodes. Zhang et al. [19] examined the effect of three organic corrosion inhibitors on the Zn electrode for Zn–MnO_2 batteries by the polarization analysis and the electrochemical impedance method. Wang et al. [20] examined the effectiveness of bismuth ion (Bi^{3+}) and tetra-butyl ammonium bromide (TBAB) for the Zn electrode to inhibit the dendritic growth in alkaline zincate solution. They found that both Bi^{3+} and TBAB had the synergistic effect on the dendritic inhibition of the Zn electrode.

* Corresponding author. Tel.: +886 2 908 4309; fax: +886 2 2904 1914.
E-mail address: ccyang@ccsun.mit.edu.tw (C.-C. Yang).

0378-7753/$ – see front matter © 2007 Elsevier B.V. All rights reserved.
doi:10.1016/j.jpowsour.2007.07.053

Usually, the electrochemical performance of a secondary Zn electrode can be studied through a galvanostatic charge/discharge method. As we know, the major effect on the electrochemical properties of a secondary Zn electrode is at the chemical composition of an electrode. In particular, only a few percent of metallic nanopowder additives, like nano-copper, CNTs, was added. In order to understand the effect of fillers on the secondary Zn electrode, a quick electrochemical characterization method needs to effectively evaluate the performance. However, using the galvanostatic charge/discharge technique to evaluate the performance of a secondary Zn electrode with different types of additives is time-consuming. In this work, we demonstrated that a fast CV method for evaluation and optimization of the chemical composition of the secondary Zn electrode can be applied. The electrochemical properties of a Zn powder electrode based on ball-milled $ZnO + Ca(OH)_2$ powders (so-called ZnCa mixture powders) was effectively investigated by using the cyclic voltammetry method. In addition, a galvanostatic charge/discharge method was also employed to examine the electrochemical properties of the secondary Zn electrodes with conductive fillers.

2. Experimental

2.1. Preparation of active materials

The active materials of the secondary Zn electrode was prepared by a mechanical ball-milled method by using ZnO (Aldrich) and $Ca(OH)_2$ (Aldrich) powders with a fix mole ratio of 2.5:1. The amounts of ZnO and $Ca(OH)_2$ raw materials were at first weighted, then mixed and put into an agate pot with 10 mm diameter agate ball. The weight ratio of the raw materials to mill ball was set at 1:5. The ball-milled pot was tightly sealed and set in a planetary ball miller (FRITSCH 7). The mechanical ball-milled treatment was carried out at a rotation speed of 300 rpm for 10 h at ambient temperature. After ball-milled treatment, the well-mixed composite oxide mixture powders were collected in a plastic container for further examination.

2.2. Composite ZnCa mixture powders characterization

The surface morphologies of the ball-milled ZnCa composite mixtures coated with a thin layer of Au were characterized by using a scanning electron microscopy (S-2600 PC-SEM made by Hitachi Co. Ltd.). The compositions of the ball-milled ZnCa mixture powders were examined by EDX mapping analysis system (RONTEC Microanalysis System, Germany). The crystal structures of ZnO, CNTs, and ZnCa mixture powders were examined using a Philips X'Pert X-ray diffractometer (XRD) with Cu Kα radiation of wavelength $\lambda = 1.54056$ Å for 2θ angles between 10° and 80°. Raman spectrum is a unique tool to characterize various active materials and conductive fillers. The Raman spectroscopy analysis was carried out by a Renishaw confocal microscopy Raman spectroscopy system with a microscope equipped with 10×, 20×, and 50× objectives, and a charge-coupled device (CCD) detector. Raman excitation source was provided by 514 nm laser beam, which had the beam power 25 mW and was focused on the sample with a spot size of about 1 μm in diameter.

2.3. Preparation of a secondary Zn electrode

The working electrode was prepared by using the ball-milled composite oxide mixture slurries; the preparation method was similar to Yang's procedure [18]. The chemical composition of a Zn powder electrode was as follows: 70 wt.% ball-milled $ZnO + Ca(OH)_2$ mixture powders, 8 wt.% Zn powders (Aldrich), 2 wt.% PbO (Aldrich), 3 wt.% Bi_2O_3 (Aldrich), 2 wt.% conductive fillers, and 15 wt.% PTFE (Du Pont, 30J) binder solution. In order to enhance the cycleability and utilization of the secondary Zn electrode, a 2 wt.% of electronic conductive fillers was chosen to add into the Zn paste slurry to replace Zn powders. Two nano-sized conductive fillers were used, such as 100 nm nano-copper powders (Aldrich) and 10–20 nm multi-wall carbon nanotubes (CNTs) (SeedChem Pty. Ltd., Taiwan). The resulting mixture slurries with those conductive fillers were further ball-milled again at a rotation speed of 300 rpm for 2 h.

The Zn powder electrode was prepared by filling a paste of mixtures of $ZnO + Ca(OH)_2$ powders into a cavity at the tip of a 1 mm Ni-plated copper electrode with a Teflon tube sheath. The construction scheme for a Zn powder electrode is shown in Fig. 1. The copper wire (Aldrich) with 1 mm diameter was at first polished with 600, 800, and 1200 grid emery papers, respectively. Then the copper wire was electroplated with a thin layer of Ni. Before it was mounted with Teflon tube, the Ni-plated copper wire was thoroughly cleaned with DI water, acetone and methanol. The geometry area of a Zn powder electrode was 0.00785 cm^2. The amount of slurry mixtures on the Zn electrode was controlled around 1–2 mg.

2.4. Electrochemical properties measurements

The cyclic voltammetry analysis of a Zn powder electrode with a mixture of $ZnO + Ca(OH)_2$ powders without or with the

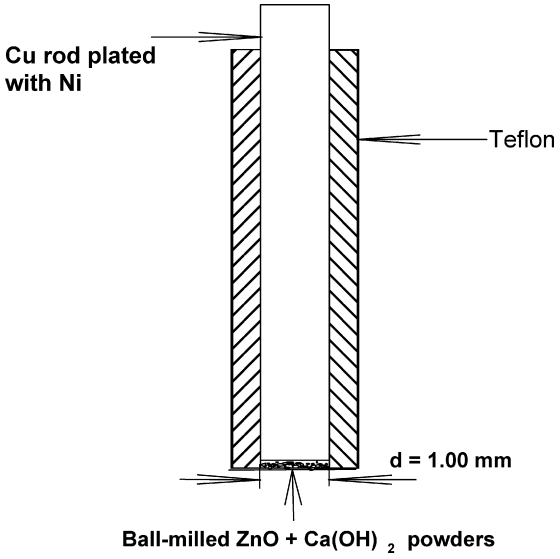

Fig. 1. The construction scheme of a Zn powder electrode.

conductive fillers was carried out on a three-electrode system. The Zn working electrode with active materials about 1–2 mg was based on ball-milled $ZnO + Ca(OH)_2$ mixtures + the electronic conductive fillers (2 wt.% nano-copper powders or 2 wt.% CNTs fillers). A large area (10 cm × 10 cm) of Pt sheet was used as the counter electrode and a Hg/HgO electrode was used as the reference electrode. All potentials were recorded versus a Hg/HgO. The electrolyte was 1 M KOH saturated ZnO. The potential sweep range was set at −1.70 to −1.0 (versus Hg/HgO) with a scan rate of 1 mV s^{-1}. A certain amount of as-prepared ball-milled $ZnO + Ca(OH)_2$ mixture powders (2.5:1), PTFE binder, and additives were mixed thoroughly. The mixture was coated into a Ni-foam substrate with an area of 1 cm × 1 cm. The chemical composition of the porous Zn electrode was as follows: 70 wt.% ball-milled $ZnO + Ca(OH)_2$ mixture powders, 8 wt.% Zn powders (Aldrich), 2 wt.% PbO (Aldrich), 3 wt.% Bi_2O_3 (Aldrich), 2 wt.% conductive fillers, and 15 wt.% PTFE (Du Pont, 30J) binder solution. The galvonostatic charge/discharge measurements were carried out on a porous Zn electrode ($A = 1\ cm^2$) wrapped with two layers Celgard 5550 PP/PE separators at a charge rate of *C*/10 and discharge rate of *C*/5. The CV and galvonostatic charge/discharge measurements were conducted by using an Autolab PGSTAT30 electrochemical system with GPES 4.8 package software (Eco Chemie, The Netherlands). All the measurements were carried out at ambient temperature.

3. Results and discussion

3.1. Characterization of active materials

Fig. 2(a) and (b) shows the SEM micrographs for the active materials of $ZnO + Ca(OH)_2$ mixtures treated with and without ball milling, respectively. It can be seen that the without ball-milled $ZnO + Ca(OH)_2$ mixtures is comprised of many larger dark $Ca(OH)_2$ particles and white tiny ZnO crystals, as shown in Fig. 2(b). By comparison with the without ball-milled treatment samples, the ball-milled $ZnO + Ca(OH)_2$ powders are much uniform and the mixture powders show many different types of plate-like crystallines of ZnO and $Ca(OH)_2$, as shown in Fig. 2(a).

Fig. 2(c) and (d) shows the SEM micrographs for the active materials of ball-milled ZnCa mixtures with 2 wt.% nano-Cu and CNTs, respectively. It was found that the CNTs fillers in ZnCa mixture powders were seen, as shown in Fig. 2(d). However, the nano-copper fillers in ball-milled ZnCa mixture powders was not distinguished clearly in SEM photograph (as shown in Fig. 2(c)).

Fig. 3(a) and (b) show the SEM image and EDX mapping (element distribution analysis) results for ball-milled $ZnO + Ca(OH)_2$ powders, respectively. Clearly, the distribution of both Zn and Ca on the ball-milled $ZnO + Ca(OH)_2$ mixture powders is random and uniform. Besides, the EDX spectrum indicates that homogeneous mixing occurs after ball milling

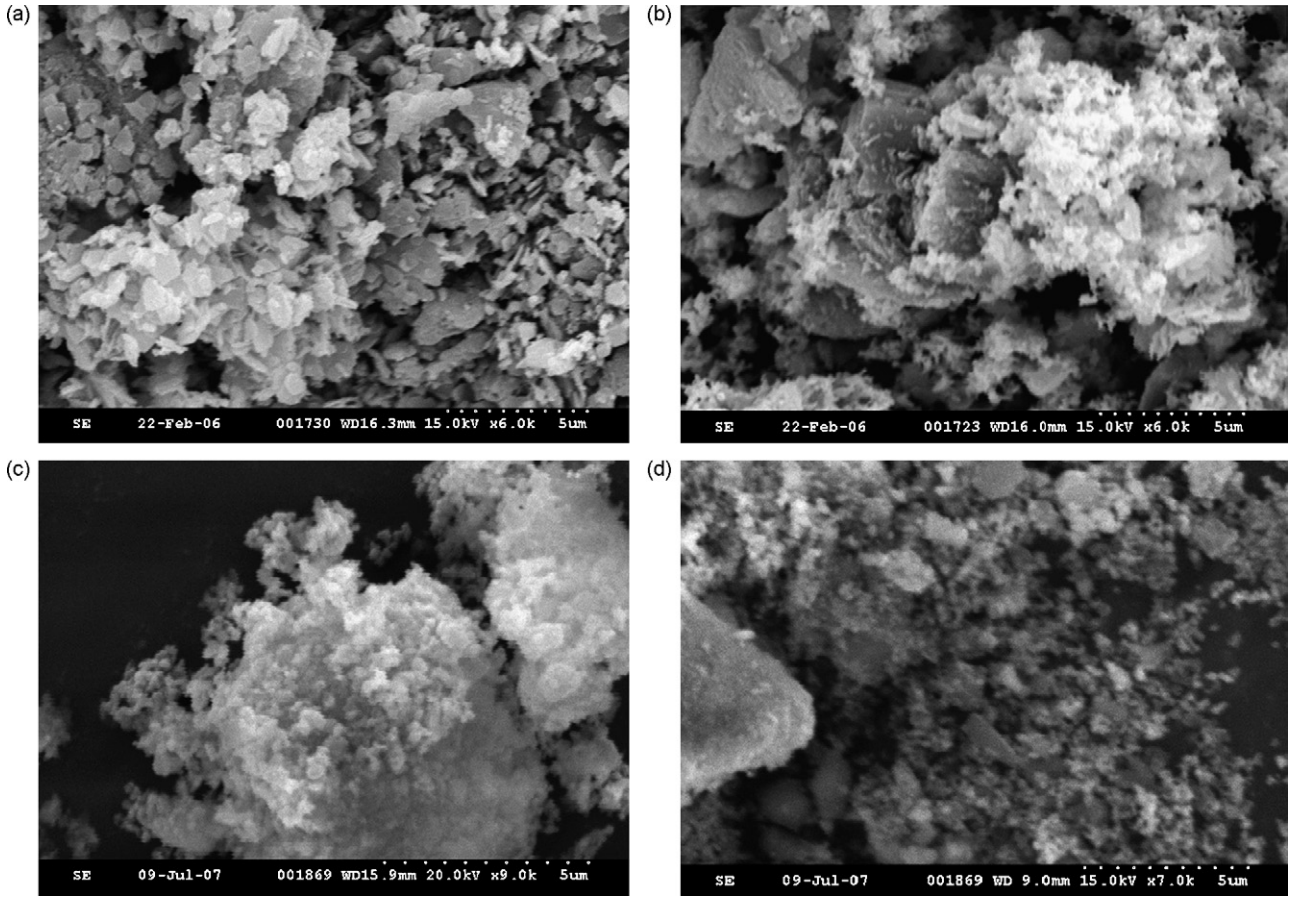

Fig. 2. SEM photographs for ZnCa mixture powders: (a) ball-milled ZnCa; (b) without ball-milled ZnCa; (c) ZnCa + 2% nano-Cu; (d) ZnCa + 2% CNTs.

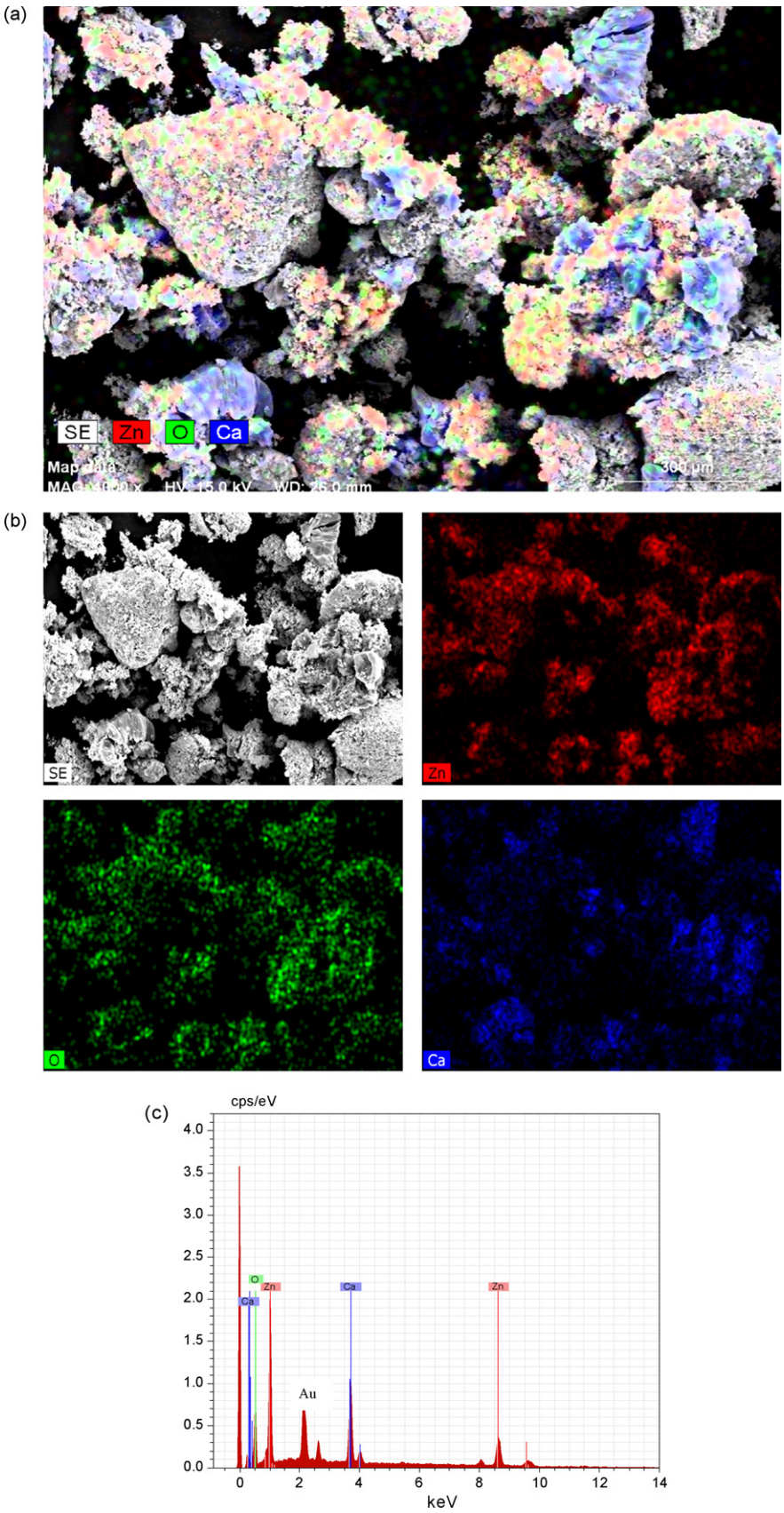

Fig. 3. SEM spectrum and EDX mapping results for ball-milled ZnCa oxide powders: (a) SEM spectrum; (b) element mapping; (c) EDX spectrum.

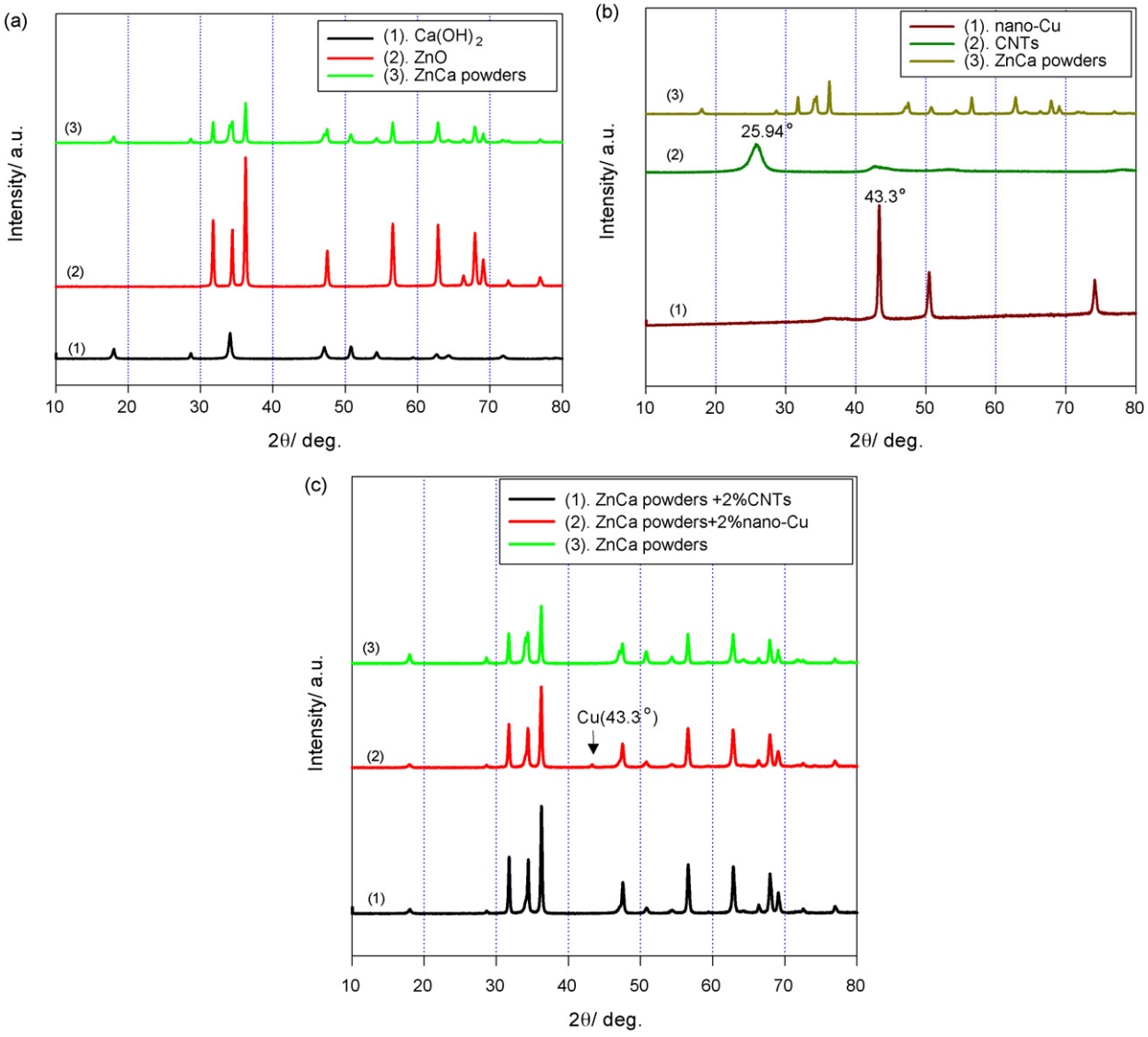

Fig. 4. XRD spectra for (a) ZnO, $Ca(OH)_2$, ball-milled ZnCa powders: (b) CNTs, nano-Cu; (c) ZnCa mixture powders + 2% conductive fillers.

because the experimental ratio of Zn to Ca is very close to the theoretical value, which we added into the miller. Therefore, the ball-milled method is a useful tool to mix ZnO and $Ca(OH)_2$ powders to form a well-mixed and uniform composition of $ZnO + Ca(OH)_2$ mixture powders.

XRD spectra of ZnO, $Ca(OH)_2$ powders and the obtained ball-milled $ZnO + Ca(OH)_2$ mixture powders are presented in Fig. 4(a). Fig. 4(b) shows XRD spectra of nano-Cu, CNTs, and the obtained ball-milled $ZnO + Ca(OH)_2$ mixture powders. Fig. 4(c) shows XRD spectra for the ball-milled ZnCa mixture powders and the ZnCa mixture powders + 2 wt.% nano-Cu and 2 wt.% CNTs, respectively. Table 1 shows all XRD's peaks for ZnO, $Ca(OH)_2$, nano-Cu, CNTs, ZnCa mixture powders and ZnCa powders + 2 wt.% conductive fillers. By comparison, the XRD spectra of ZnO, $Ca(OH)_2$ powders and ZnCa powders all displays in Fig. 4(a). It can be clearly seen that the ball-milled treatment does not alter the basic crystal structures of raw materials of ZnO and $Ca(OH)_2$ powders. However, the intensities of major peaks in the XRD spectra of the ball-milled ZnCa mixture powders are reduced and much broadened. According to the Scherrer's formula, i.e., $d = 0.9\lambda/B\,cos(\theta)$, where d is the crystalline size, λ the X-ray wavelength, B the full width of half-maximum (FWHM) intensity, and θ is the Bragg angle. The crystal size of d is inversely proportional to the B value, so the XRD peak is broadened, which implied that the crystalline size of the ball-milled mixtures becomes smaller, compared to the non-ball-milled $ZnO + Ca(OH)_2$ mixtures.

As seen clearly in Fig. 4(c), it was found that a very small XRD peak at $2\theta = 43.30^\circ$ for nano-Cu materials was detected for the ball-milled ZnCa mixture powders + 2 wt.% nano-Cu fillers. However, we did not found any XRD peak for CNTs fillers. Thus, the physical mechanical ball-milled method is an effective tool to prepare a uniform of $ZnO + Ca(OH)_2$ mixture powders; in particular, it can be used to prepare the active materials with the additional conductive fillers for a secondary Zn electrode.

Moreover, Raman analysis can also qualitatively examine the composition of ZnCa mixture powders + conductive fillers. Fig. 5(a) shows the Raman spectra for ZnO, $Ca(OH)_2$, and

Table 1
XRD test results for ZnO, $Ca(OH)_2$ and nano-Cu powders, ball-milled ZnCa mixture powders + conductive fillers

Species	Peak positions (°)
$Ca(OH)_2$	18.06, 28.66, 34.10, 47.10, 50.78, 54.34, 62.66, 64.34, 71.86, 76.94
ZnO	31.74, 34.42, 36.22, 47.54, 56.58, 62.86, 66.38, 67.94, 69.06
Nano-Cu	36.82, 43.34, 50.54, 74.14
CNTs	25.94, 42.82, 53.06, 78.10
ZnCa powders	18.02, 31.74, 34.06, 34.14, 34.38, 36.22, 47.10, 47.50, 50.78, 62.86, 69.06, 76.94
ZnCa powders + 2 wt.% nano-Cu	17.98, 28.66, 31.74, 34.38, 36.26, 43.30, 47.50, 50.82, 54.34, 56.58, 62.82, 66.42, 67.94, 69.10, 74.18, 76.94
ZnCa powders + 2 wt.% CNTs	31.78, 34.46, 36.26, 47.54, 56.62, 62.86, 66.38, 67.94, 69.10, 77.02

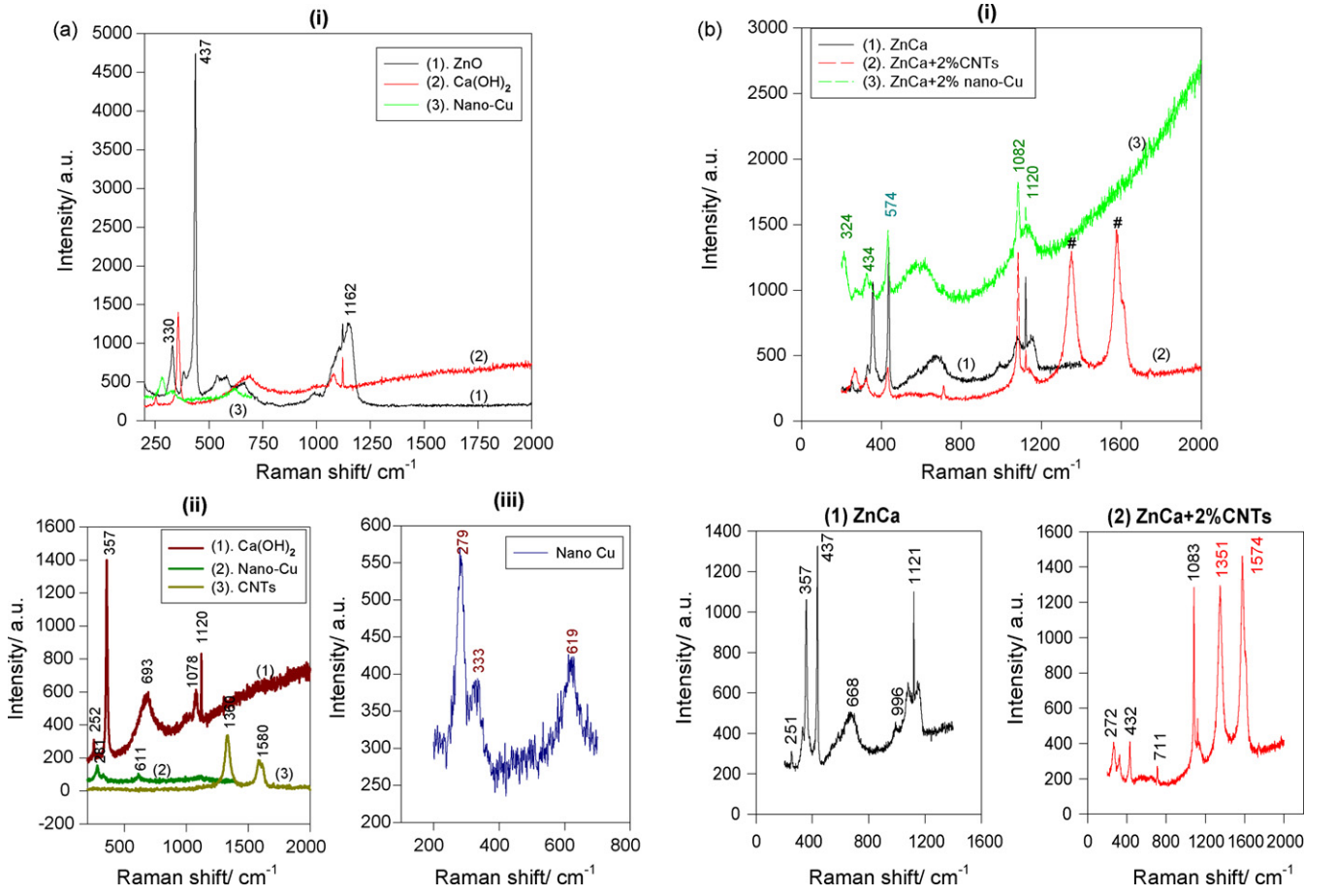

Fig. 5. Raman spectra for (a) ZnO, $Ca(OH)_2$ powders, nano-Cu powders: (b) ball-milled ZnCa powders + 2%fillers.

nano-Cu powders. Table 2 lists the major peaks of ZnO, $Ca(OH)_2$, and nano-Cu powders. There are three main peaks for ZnO, i.e., at 330, 437 and 1162 cm^{-1} [21,22]. But, there are four major Raman peaks for $Ca(OH)_2$, namely, at 252, 357, 693 and 1078 cm^{-1}. In particular, three small Raman peaks for nano-Cu powders (those peak bands may be due to the formation of oxides on the surface of copper particles) are located at 279, 333 and 619 cm^{-1}. Fig. 5(b) also shows the Raman spectra for ZnCa mixture powders, ZnCa mixture powders + 2 wt.% nano-Cu and CNTs fillers, respectively. Table 3 also lists the major peak bands for ZnCa mixture powders, ZnCa mixture powders + 2 wt.% nano-Cu and CNTs fillers. Obviously, for ball-milled ZnCa mixture powders + 2 wt.% CNTs fillers, there are six major Raman peaks, i.e., at 272, 432, 711, 1083, 1351 and 1574 cm^{-1}. The Raman spectra with those peaks at 1351 (D-band, for amorphous phase) and 1574 cm^{-1} (G-band, for crystalline phase) [23] indicate that the CNTs fillers were homogeneously mixed into ZnO and $Ca(OH)_2$ compounds.

Table 2
Raman results for ZnO, $Ca(OH)_2$, nano-Cu powders, and CNTs fillers

Species	Raman peaks (cm^{-1})
ZnO	330, 437, 1162
$Ca(OH)_2$	252, 357, 693, 1078
Nano-Cu	279, 333, 619
CNTs	1360, 1580

Table 3
Raman results for ball-milled ZnCa powders and ZnCa powders + fillers

Species	Raman peaks (cm^{-})							
ZnCa powders	251	357	437	668	996	1121	—	—
ZnCa + 2% CNTs	272	—	432	711	1083	—	1351	1574
ZnCa + 2% nano-Cu	—	324	434	574	1082	—	—	—

3.2. The CV analyses of the Zn powder electrodes

The electrochemical properties of the Zn powder electrode can be effectively evaluated by cyclic voltammetry (CV) method. The parameters obtained from the CV's result are the anodic peak potential ($E_{p,a}$), the anodic peak current density ($i_{p,a}$), the cathodic peak potential ($E_{p,c}$), the cathodic peak current density ($i_{p,c}$). At the same time, the peak separation ($\Delta E_{a,c}$), which is defined as the difference between the anodic peak potential and the cathodic peak potential ($\Delta E_{a,c} = |E_{p,a} - E_{p,c}|$); which is a measure of reversibility of the electrode (redox pair) reaction. Accordingly, the smaller the value of $\Delta E_{a,c}$, the more the thermodynamic reversible of the electrode reaction. Moreover, the anodic discharge capacity (Q_{dis}) and the cathodic charge capacity (Q_{ch}), and the current efficiency (CE (%)), which is defined as $CE(\%) = Q_{dis}/Q_{ch} + 100\_$ can be calculated. Finally, the R, it is defined as $R = i_{p,a}/i_{p,c}$, which is defined as the ratio of the anodic to cathodic peak heights, also can be obtained; it may represent the reversibility of the porous Zn electrode.

It has been widely accepted that a small amount of organic surfactants [12–15] or metallic conductive fillers or additives [9,10] played a crucial effect on the charge/discharge properties. These parameters of CV can be offered to evaluate effectively the electrochemical properties of the Zn electrodes when a small amount of conductive fillers is added into the electrode.

Fig. 6 shows the typical cyclic voltammograms of the Zn powder electrode based on ball-milled $ZnO + Ca(OH)_2$ mixture powders without any conductive fillers at different cycles in 1 M KOH saturated ZnO solution at a scan rate of 1 mV s^{-1} at 25 °C. As a result, it can be clearly seen from Fig. 6 that the cathodic and anodic peaks of a porous Zn electrode are more separable and much clearer; however, the CV curves are stable during the forward and the reverse scanning directions.

Accordingly, as shown in inset of Fig. 6, there are two cathodic and two anodic peaks on the 50th cyclic voltammograms, one large anodic peak ($I_{p,a}$) is at −1.19 V for the anodic oxidation of a mixture of $ZnO + Ca(OH)_2$ compounds [14] and the other is a small anodic hump peak ($II_{p,a}$) at about −1.21 V for

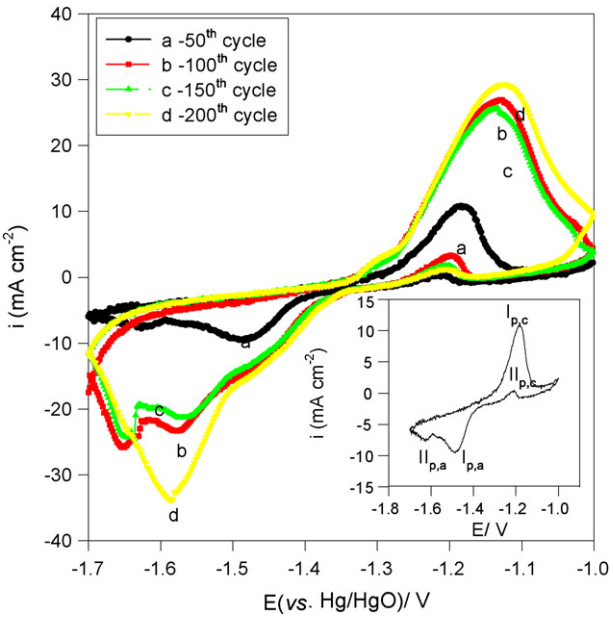

Fig. 6. The cyclic voltammograms of a porous Zn electrode based on ball-milled $ZnO + Ca(OH)_2$ powders in 1 M KOH saturated ZnO with a scan rate of 1 mV s^{-1}; the inset, at the 50th cycle of CV.

the re-oxidation of Zn to ZnO in the reverse scan direction. Conversely, there are also two cathodic peaks, one major cathodic peak ($I_{p,c}$) is at about −1.49 V for the reduction of a mixture of $ZnO + Ca(OH)_2$ compounds, the other peak ($II_{p,c}$) is at −1.63 V for the reduction of ZnO or $Zn(OH)_2$. During the scanning, the anodic and cathodic peaks gradually increase; the reason for this enhancement performance of a porous Zn electrode may be due to the good cycleability of a mixture of $ZnO + Ca(OH)_2$ powders [6,16–18]. Table 4 also displays the CV's parameters of a porous Zn electrode without any filler at different number cycles. It was found that the discharge capacity of a porous Zn electrode based on ball-milled $ZnO + Ca(OH)_2$ mixture powders without any conductive filler gradually declined; but the CV curves are still stable during 200 charge/discharge cycle tests.

Table 4
The parameters from the CV results for a Zn powder electrode without fillers

Cycles	Q_{dis} (mC)	$-Q_{ch}$ (mC)	CE (%)	$E_{p,a}$ (V)	$E_{p,c}$ (V)	$\Delta E_{a,c}$ (V)	$-i_{p,c}$ (mA cm^{-2})	$i_{p,a}$ (mA cm^{-2})	R
50	14.1	34.5	40.87	−1.17	−1.64	0.470	10.2	7.53	0.74
100	21.5	33.0	65.16	−1.13	−1.57	0.440	26.7	23.1	0.87
150	36.4	53.1	68.59	−1.13	−1.56	0.430	25.6	21.2	0.83
200	44.5	61.9	71.78	−1.13	−1.63	0.500	29.2	25.4	0.87

Note: $\Delta E_{a,c} = E_{p,a} - E_{p,c}$, $R = -i_{p,a}/i_{p,c}$. $CE = Q_{dis}/Q_{ch}$ (where Q_{dis} is the discharge capacity and Q_{ch} is the charge capacity).

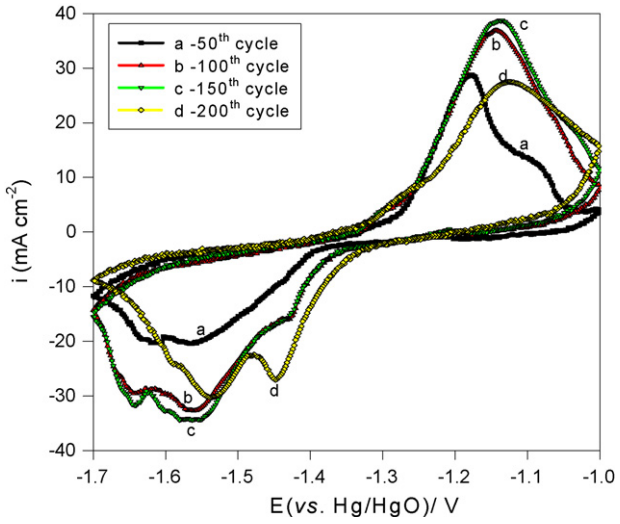

Fig. 7. The cyclic voltammograms of a porous Zn electrode based on ball-milled ZnO + $Ca(OH)_2$ powders + 2 wt.% nano-copper in 1 M KOH saturated ZnO at a scan rate of 1 mV s^{-1}.

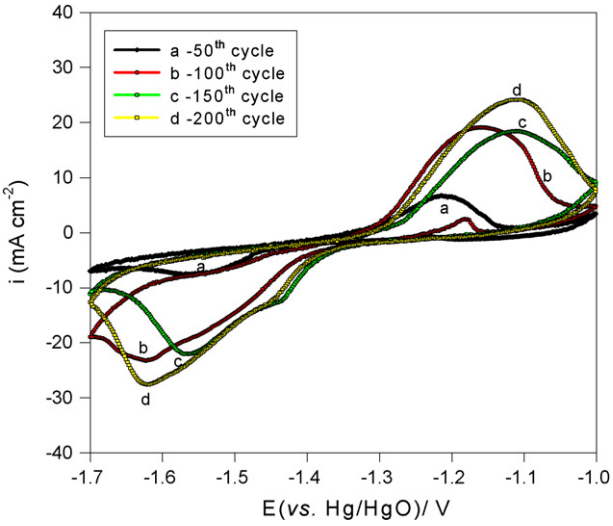

Fig. 8. The cyclic voltammograms of a porous Zn electrode based on ball-milled ZnO + $Ca(OH)_2$ powders + 2 wt.% CNTs in 1 M KOH saturated ZnO at a scan rate of 1 mV s^{-1}.

3.3. The CV analyses for the Zn powder electrode with nano-sized copper fillers

Fig. 7 shows the cyclic voltammograms of the Zn powder electrode based on ball-milled ZnO + $Ca(OH)_2$ mixture powders + 2 wt.% nano-sized copper conductive fillers at various cycles in 1 M KOH saturated ZnO solution at a scan rate of 1 mV s^{-1} at 25 °C. It can certainly be observed that two cathodic peaks and one anodic peak of a porous Zn electrode are well defined; but the CV curves are rather smooth and stable during the discharge and the charge cycles. Whereas, one major anodic peak is at −1.20 to −1.15 V and two cathodic peaks are at −1.45 to −1.55 V and at −1.55 to −1.65 V on the cyclic voltammograms. Table 5 lists the CV's parameters for a porous Zn electrode with nano-sized copper filler at various cycles. Apparently, it was found that the discharge capacity and cycleability of a secondary Zn electrode with the nano-copper fillers is greatly enhanced through 200 cycle tests.

Comparatively, it was discovered that the anodic peak current density ($i_{p,a}$ about 20–34 mA cm^{-2}) and the cathodic peak current density greatly increased after 100–200 cycle tests, compared with that of the Zn powder electrode without conductive fillers ($i_{p,a}$ about 7–25 mA cm^{-2}). In addition, the maximum anodic discharge capacity ($Q_{dis,}$) of the Zn powder electrode was reached about 52.6 mC, with a CE of 75%, and with the value of R (R defined as $-i_{p,a}/i_{p,c}$) of 0.90–0.91. These CV results indicate that the Zn powder electrodes with nano-sized copper conductive fillers show indeed better reversibility and electrochemical performances. Accordingly, the shape change and the dendritic formation of the secondary Zn electrode can be reduced due to the two effects of the calcium zincate mixtures (Ca greatly reduces the solubility of the Zn electrode in KOH solution) and the nano-sized conductive fillers (they enhance electronic conductivity property).

3.4. The CV analyses for the Zn powder electrode with CNTs fillers

Fig. 8 also shows the cyclic voltammograms of the Zn powder electrode based on ball-milled ZnO + $Ca(OH)_2$ mixture powders + 2 wt.% CNTs fillers at various cycles in 1 M KOH saturated ZnO solution at a scan rate of 1 mV s^{-1} at 25 °C. It can be observed that the two cathodic peaks and one anodic peak for this Zn powder electrode are well-defined; but the CV curves are slightly broadened, these peaks are not well-defined or sharp during the forward and the reverse scanning. Apparently, there is one major anodic peak at −1.1 to −1.2 V and two major cathodic peaks at −1.45 V and about −1.56 to −1.62 V, respectively. Table 6 also lists the CV's parameters for the Zn powder electrode plus 2 wt.% CNTs fillers at various cycles. In fact, it was found that the major anodic peak current densities ($i_{p,a}$ about 18–24 mA cm^{-2}) of the Zn powder electrode with 2 wt.% CNTs fillers are comparable with that of the Zn powder electrode free of conductive additives ($i_{p,a}$ about 21–23 mA cm^{-2}).

Additionally, the maximum discharge capacity of the Zn powder electrode with 2 wt.% CNTs fillers is about 38.2 mC, a CE

Table 5
The parameters from the CV results for a Zn powder electrode with 2 wt.% Cu fillers

Cycles	Q_{dis} (mC)	$-Q_{ch}$ (mC)	CE (%)	$E_{p,a}$ (V)	$E_{p,c}$ (V)	$\Delta E_{a,c}$ (V)	$-i_{p,c}$ (mA cm^{-2})	$i_{p,a}$ (mA cm^{-2})	R
50	31.3	50.9	61.49	−1.18	−1.56	0.380	28.7	20.4	0.71
100	51.8	75.3	68.79	−1.14	−1.56	0.420	36.9	32.6	0.88
150	52.6	70.3	74.82	−1.14	−1.56	0.420	38.2	34.4	0.90
200	48.9	64.9	75.35	−1.13	−1.54	0.410	30.1	27.3	0.91

Table 6
The CV results for a Zn powder electrode with 2 wt.% CNTs fillers

Cycles	Q_{dis} (mC)	$-Q_{ch}$ (mC)	CE (%)	$E_{p,a}$ (V)	$E_{p,c}$ (V)	$\Delta E_{a,c}$ (V)	$-i_{p,c}$ (mA cm^{-2})	$i_{p,a}$ (mA cm^{-2})	R
50	8.2	25.1	32.67	−1.21	−1.54	0.330	7.38	6.74	0.91
100	29.9	60.6	49.34	−1.17	−1.62	0.450	22.7	18.9	0.83
150	37.3	53.6	69.60	−1.14	−1.63	0.490	23.9	17.5	0.73
200	38.2	59.5	64.20	−1.12	−1.62	0.500	27.3	24.0	0.88

of 64%, and the R value at 0.73–0.88. It was found that the electrochemical performance of the porous Zn electrode with CNTs fillers shows slightly better than that of the Zn powder electrode without conductive fillers only after 100 cycle test. However, the result indicates that the long-term cycleability of the Zn electrode can only be improved to some extent by the CNTs fillers. In conclusion, the electrochemical and cycleability performances for the Zn powder electrode with the CNTs fillers can be improved slightly.

3.5. Comparisons of the CV's results for the Zn powder electrodes

Fig. 9 shows the plot of the total discharge capacities (Q_{dis}) versus the number cycle of different Zn powder electrodes. It can be seen from Fig. 9 that the total discharge capacities of the Zn powder electrodes with the conductive fillers were greatly increased (max. about 52.6 mC) when the number cycles of the CV test are increased. But, the total discharge capacity of the Zn powder electrode without conductive fillers is much lower (max. about 44.5 mC). While, it is obvious that the nano-sized conductive fillers, have greatly influenced on the discharge capacity properties of secondary Zn powder electrode due to their high surface area and good electronic conductivity (the electronic conductivity for $\sigma_{Cu} \sim 10^5$ S cm^{-1} and $\sigma_{CNT} \sim 10^2$ S cm^{-1}).

Fig. 10 shows a plot of current efficiency CE (%) versus the number cycle for the various Zn powder electrodes. It was found that the current efficiencies of the Zn electrodes with those conductive fillers were gradually increased as the number cycles of CV test were increased. As a matter of fact, the current efficiency of the Zn electrode without any conductive filler is about 68–71% after 200 cycle tests. In particular, the CE (%) of the Zn electrode with 2 wt.% nano-copper filler is increased; it is about 75% after 200 cycles. Comparatively, the current efficiency of the Zn powder electrode with 2 wt.% CNTs (CE (%) about 69%) is comparable with that of the Zn powder electrode without filler (CE (%) about 68–71%) after 200 cycling tests. Moreover, the R values of all Zn powder electrodes with and without fillers are at a range of 0.8–0.9. Finally, the $\Delta E_{a,c}$ values are only as high as 0.4–0.5, which implies that the reversibility of the Zn powder electrode is still not satisfied. It may be due to the high bulk resistance for the Zn powder electrode containing large amounts of non-conductive ZnO and $Ca(OH)_2$ materials, as compared with a planar bulk Zn electrode.

3.6. The galvonostatic charge/discharge measurements

Fig. 11(a) and (b) shows the charge and discharge (E–t) potential curves of the porous Zn electrode with a geometry area of 1 cm^2 (without conductive fillers) at a charge rate of C/10 and a discharge rate of C/5 at 1–5 and 6–10 cycles, respectively. It can be seen from Fig. 11(a) and (b) that the charge potential curves of the Zn porous electrodes without conductive fillers were greatly polarized to the negative direction due to poor electronic

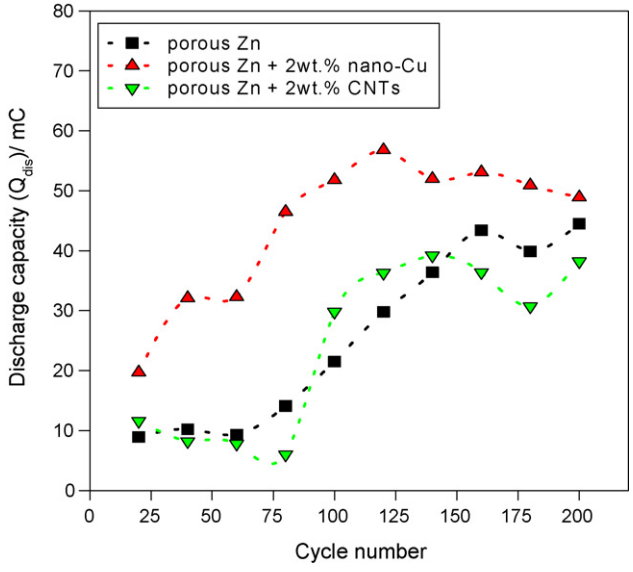

Fig. 9. The plot of anodic discharge capacity vs. the number cycles for different porous Zn powder electrodes.

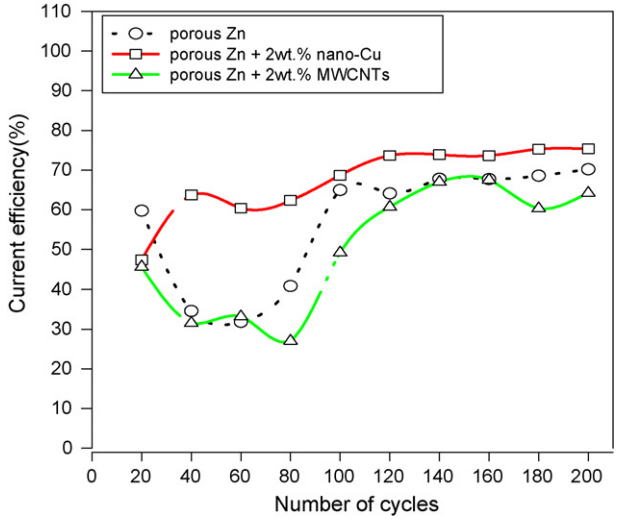

Fig. 10. The plot of current efficiency (%) vs. cycle number for different porous Zn powder electrodes.

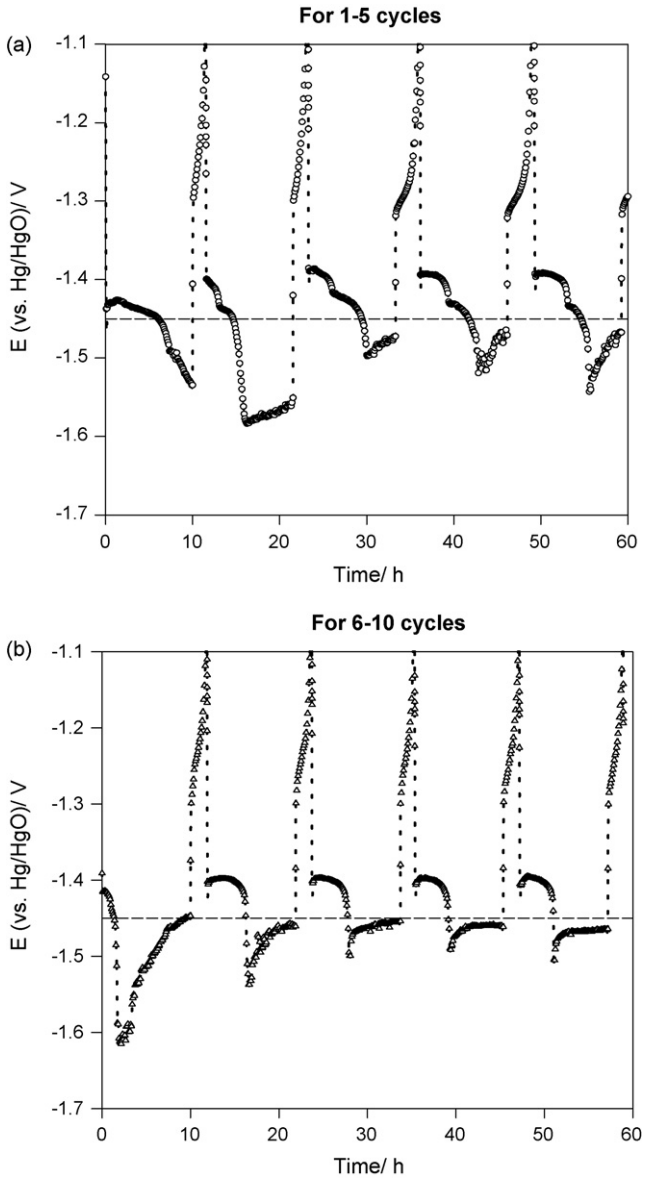

Fig. 11. The *E–t* curves of a porous Zn electrode based on ball-milled ZnO + $Ca(OH)_2$ (charge at *C*/10 and discharge at *C*/5).

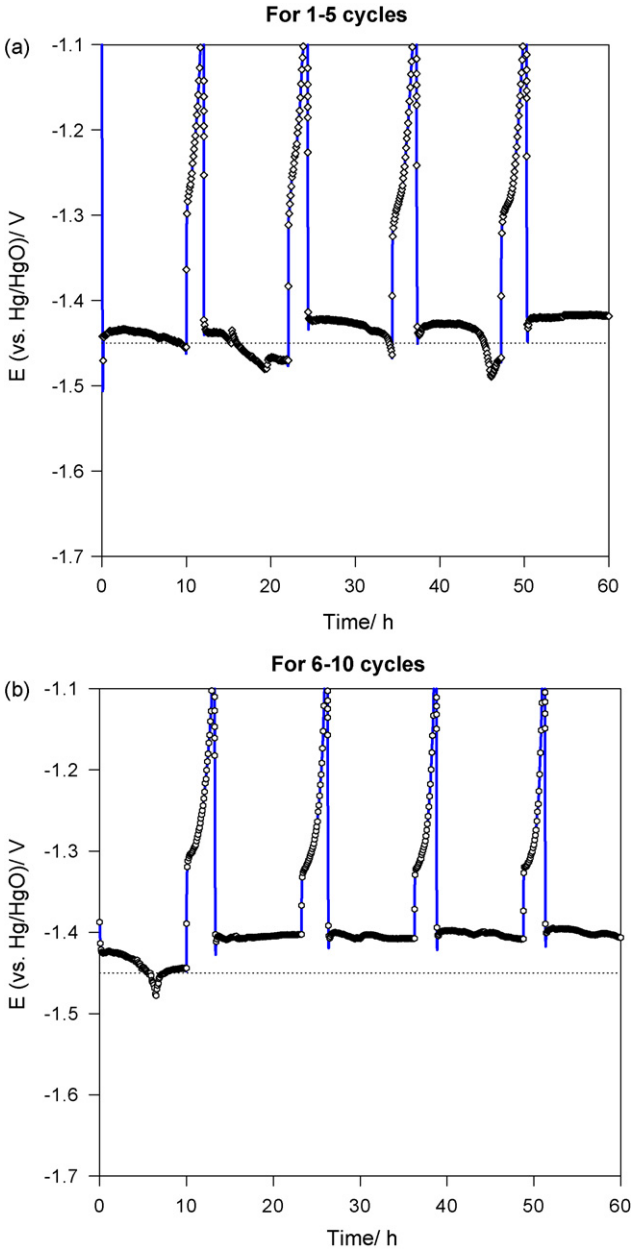

Fig. 12. The *E–t* curves of a porous Zn electrode based on ball-milled ZnO + $Ca(OH)_2$ mixture powders + 2 wt.% nano-Cu (charge at *C*/10 and discharge at *C*/5).

conductivity (high bulk resistance and easily produce H_2 gas) of ZnO and $Ca(OH)_2$ mixtures. In fact, the electrode potential during the charge is also not stable and it highly varied at a potential of between −1.5 and −1.6 V (versus Hg/HgO).

Fig. 12(a) and (b) shows the charge and discharge (*E–t*) potential curves of the porous Zn electrode with 2 wt.% nano-sized Cu fillers at a charge rate of *C*/10 and a discharge rate of *C*/5 at 1–5 and 6–10 cycles, respectively. It can be seen clearly that the charge potential of the Zn electrode with copper conductive fillers is much flat and stable. This may be due to the enhancement of electronic conductivity of the Zn electrode with nano-Co powders. The charge potential is stable and it varied between −1.4 and −1.45 V (versus Hg/HgO). The polarization of the porous Zn electrode at the charge condition is much less; therefore, the current efficiency and the cycle life can be improved.

Fig. 13 shows the discharge potential curves of the porous Zn electrode with 2 wt.% nano-Cu fillers at a discharge rate of *C*/5 (with theoretical capacity Q_{theo} = 115 mAh) at different cycles (1–50 cycles). As a result, the discharge potential of the porous Zn electrode is much stable and flat around −1.310 V (versus Hg/HgO), the number cycles of charge/discharge tests extend to over 50 cycles. The highest discharge capacity for the as-prepared porous Zn electrode (A = 1 cm^2) is at the 30th cycle. Clearly, the discharge capacity is declined quickly after over 30 cycles, the real discharge capacity was only about half of theoretical capacity (only about 50 mAh) at the 50th cycle (i.e., the discharge time about 2.5 h).

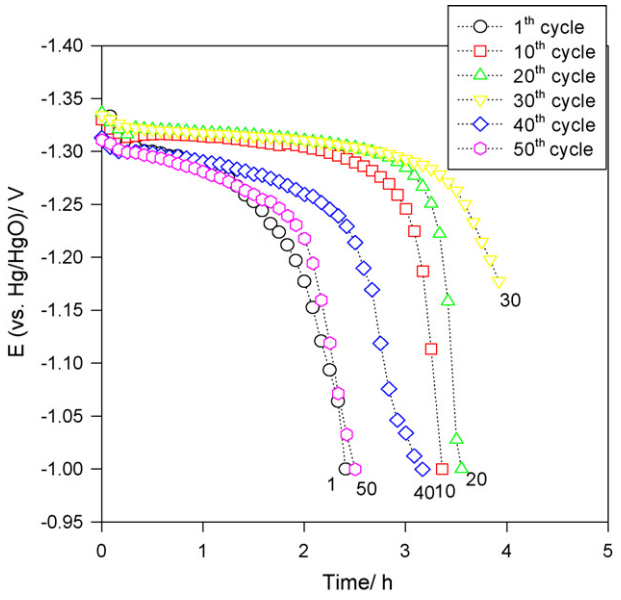

Fig. 13. The discharge curves of a porous Zn electrode based on ball-milled ZnO + $Ca(OH)_2$ mixture powders + 2 wt.% nano-Cu fillers at different cycles (charge at *C*/10 and discharge at *C*/5 rates).

4. Conclusions

The active materials of the secondary Zn electrode containing ZnO and $Ca(OH)_2$ mixture powders was prepared by a ball-milled treatment. The electrochemical properties of the Zn electrodes + 2 wt.% nano-Cu and CNTs conductive fillers were systematically examined by using the cyclic voltammetry method and the galvonostatic charge/discharge test. Using both XRD and micro-Raman spectroscopy methods can analyze the compositions of nano-Cu and CNTs conductive fillers in the ball-milled ZnCa mixture powders.

Whereas the electrochemical parameters obtained from the CV, such as Q_{dis}, Q_{ch}, $E_{p,a}$, $i_{p,a}$, $E_{p,c}$, $i_{p,c}$, CE, R, $\Delta E_{a,c}$, etc., can be obtained to optimum the chemical composition of a secondary Zn electrode. It was experimentally found that the electrochemical properties and the cycle life of the secondary Zn electrode could be improved after both the $Ca(OH)_2$ compound and the conductive fillers were added together. The galvonostatic charge/discharge tests were also conducted for a porous Zn electrode. The results of the galvonostatic charge/discharge tests are well consistent with that of the CV tests. The cycle life of the secondary Zn electrode was extended to over 50 cycles. The CV technique here offers a quick electroanalytical method to effectively evaluate the performance of the secondary Zn electrode. Especially, there are only a few percents of the additive fillers added into the electrode.

Acknowledgement

Financial support from the Taiwan Power Company, Taiwan (Project No.: TPC-546-4311-9401B) is gratefully acknowledged.

References

[1] J.W. Evans, G. Savaskan, J. Appl. Electrochem. 21 (1991) 105.
[2] G. Savaskan, T. Huh, J.W. Evans, J. Appl. Electrochem. 22 (1992) 909.
[3] T. Huh, G. Savaskan, J.W. Evans, J. Appl. Electrochem. 22 (1992) 916.
[4] J.C. Salas-Morales, J.W. Evans, J. Appl. Electrochem. 24 (1994) 858.
[5] H. Yang, Y. Cao, X. Ai, L. Xiao, J. Power Sources 128 (2004) 97.
[6] C. Zhang, J.M. Wang, L. Zhang, C.N. Cao, J. Appl. Electrochem. 31 (2001) 1049.
[7] S. Muller, F. Holzer, O. Haas, J. Appl. Electrochem. 28 (1998) 895.
[8] M.G. Chu, J. McBreen, G. Adzic, J. Electrochem. Soc. 128 (11) (1981) 2281.
[9] B.T. Hang, M. Eashira, I. Watanabe, S. Okada, J.I. Yamaki, S.H. Yoon, I. Mochida, J. Power Sources 143 (2005) 256.
[10] F.R. McLarnon, E.J. Cairns, J. Electrochem. Soc. 139 (1991) 645.
[11] H. Yang, X. Meng, E. Yang, X. Wang, Z. Zhou, J. Electrochem. Soc. 151 (3) (2004) A389.
[12] Y. Ein-Eli, M. Auinat, D. Starsvetsky, J. Power Sources 114 (2003) 330.
[13] Y. Ein-Eli, Electrochem. Solid-State Lett. 7 (1) (2004) B5.
[14] Y. Ein-Eli, M. Auinat, J. Electrochem. Soc. 150 (12) (2003) A1606.
[15] Y. Ein-Eli, M. Auinat, J. Electrochem. Soc. 150 (12) (2003) A1614.
[16] X.M. Zhu, H.-X. Yang, X.-P. Ai, J.-X. Yu, Y.-L. Cao, J. Appl. Electrochem. 33 (2003) 607.
[17] H. Yang, H. Zhang, X. Wang, J. Wang, X. Meng, Z. Zhou, J. Electrochem. Soc. 151 (12) (2004) A2126.
[18] J. Yu, H. Yang, X. Ai, X. Zhu, J. Power Sources 103 (2001) 93.
[19] D. Zhang, L. Li, L. Cao, N. Yang, C. Huang, Corros. Sci. 43 (2001) 1627.
[20] J.M. Wang, L. Zhang, C. Zhang, J.Q. Zhang, J. Power Sources 102 (2001) 139.
[21] S. Music, D. Dragcevic, S. Popovic, M. Ivanda, Mater. Lett. 59 (2005) 2388.
[22] S.J. Chen, Y.C. Liu, Y.M. Lu, J.Y. Zhang, D.Z. Shen, X.W. Fan, J. Cryst. Growth 289 (2006) 55.
[23] Z.G. Huang, Z.P. Guo, A. Calka, D. Wexler, H.K. Liu, J. Alloys Compd. 427 (2007) 94.